


Measuring angular rotation via the rotatory dispersion effect

Chongqi Zhou,^{1,2} Suyi Zhong,² Kaijie Ma ^{1,2} Yang Xu,² Lixuan Shi,^{1,2} and Yonghong He^{1,2,*}

¹*Department of Physics, Tsinghua University, Beijing 100084, China*

²*Institute of Optical Imaging and Sensing, Shenzhen Key Laboratory for Minimal Invasive Medical Technologies, Graduate School at Shenzhen, Tsinghua University, Shenzhen 518055, China*



(Received 13 March 2020; accepted 1 December 2020; published 22 December 2020)

We propose a scheme for an ultrasensitive weak measurement system with an ultrasensitive rotatory dispersion effect to measure angular rotation. Estimation of angular rotation is obtained by the shift of the center wavelength. In our scheme, we obtain a continuously adjustable coupling strength and show that our system provides a 13 times higher sensitivity of 38 840 nm/rad compared with previous work. Here we demonstrate that our scheme may offer an optimal weak value A_w in practice and outperforms conventional measurements in the presence of technical noise. The precision achieved by optimized weak value amplification (WVA) is about three times higher than that of a polarimeter. Our work extends the working regime of WVA. Its simplicity and robustness clear the way for widespread use of WVA involving measurements with commercial cameras and small signals.

DOI: [10.1103/PhysRevA.102.063717](https://doi.org/10.1103/PhysRevA.102.063717)

I. INTRODUCTION

Polarization plays an important role in modern science. Nowadays high-precision polarization measurement has been widely applied in many fields, such as plasma [1], condensed matter [2], and quantum optics [3]. In particular, optical rotation (OR) measurements have drawn much attention [2,4–6]. The standard tool is photoelastic polarization modulation technology [7], which requires a laser source and photoelastic modulator. Compared with a conventional polarimeter [8], it achieves a much higher precision up to 10^{-7} rad. However, the precision is still limited by noise and systematic errors.

Weak value amplification (WVA), proposed by Aharonov [9], has attracted extensive attention in precision metrology. This metrological technique is based on a weak value under properly chosen preselection and postselection, which leads to significant amplification for parameter estimation. In 2008, Hosten and Kwiat [10] verified the utility of weak-value amplification with respect to standard measurement by attaining sensitivity to displacements of 1 Å. After that, based on WVA technology, ultrasensitive measurements of tiny physical parameters were experimentally achieved, such as velocity [11], phase estimation [12], and optical nonlinearity [13]. Significant work shows the robustness of WVA against technical noise [14–17]. Analogously, the anomalous amplification of WVA technology has also been introduced to OR detection [18]. These experiments analyze displacements of beam deflection via the spin Hall effect in weak measurement. In our previous work, two kinds of schemes were proposed to detect OR via weak measurement [19,20]. A wavelength plate and phase modulator were introduced in both schemes to produce interaction between the polarization state and light frequency. In the frequency spectrum, they achieved a sensi-

tivity of 2880 nm/rad. However, a much better performance cannot be expected for those two systems. As Xu [12] pointed out, higher sensitivity is accompanied with smaller coupling strength. For these systems, the phase difference between two orthogonal linear polarization is set as an integer multiple of π , which sets a limit on the coupling strength [12,21].

In this work, we propose an ultrasensitive scenario to investigate optical rotation via weak measurement in the frequency domain. Compared with our previous systems via weak measurement, our system removes the birefringent crystal, like a wavelength plate, phase modulator, or photoelastic modulator, and introduces a rotatory dispersion effect to generate the coupling between the light frequency and polarization state. A 13 times higher sensitivity of 38 840 nm/rad is obtained in our system. We prove that optimized WVA can overperform conventional measurement (CM) when the system is limited by light intensity jitter.

II. THEORETICAL FRAMEWORK

In quantum mechanics, for the system with a state $|\psi_i\rangle$, the mean value for an observable \hat{A} in a strong measurement is written as $\langle \hat{A} \rangle = \langle \psi_i | \hat{A} | \psi_i \rangle / \langle \psi_i | \psi_i \rangle$. The value of $\langle \hat{A} \rangle$ lies between the eigenvalues. However, Aharonov and his collaborators [9] introduced an alternative formation for quantum measurement theory: $A_w = \langle \psi_f | \hat{A} | \psi_i \rangle / \langle \psi_f | \psi_i \rangle$. They call A_w the weak value of observable \hat{A} in the system, which is preselected in $|\psi_i\rangle$ and postselected in $|\psi_f\rangle$. If the state $|\psi_i\rangle$ and $|\psi_f\rangle$ are almost orthogonal and $|\psi_i\rangle$ or $|\psi_f\rangle$ is not one of the eigenstates of \hat{A} , A_w generally goes beyond the range of the eigenvalues. This abnormal phenomenon would lead to an amplification of the signal.

In weak measurement scenario, we focus on high-sensitivity parameter estimation. Generally we couple the system and pointer with Hamiltonian $\hat{H} = \tau \delta(t - t_0) \hat{\mathbf{P}} \otimes \hat{\mathbf{A}}$, where $\hat{\mathbf{A}}$ represents the operator of the system and $\hat{\mathbf{P}}$

*heyh@sz.tsinghua.edu.cn

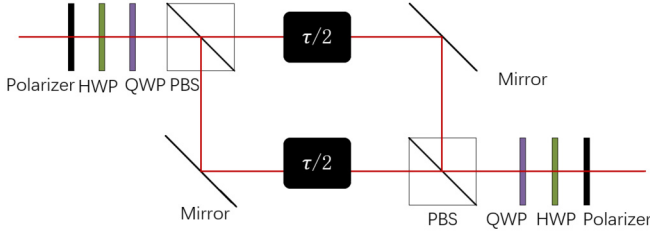


FIG. 1. Mach-Zehnder interferometer for small time delay τ between two arms. The incoming light is linear polarized and then split by PBS into two arms with two linear polarizations $|H\rangle$ and $|V\rangle$. Transformation between $\{|\psi_r^+\rangle, |\psi_r^-\rangle\}$ and $\{|H\rangle, |V\rangle\}$ can be realized through a half-wave plate (HWP) and a quarter-wave plate (QWP). The light is recombined at the second PBS, and the postselection procedure is realized through the latter polarizer.

represents the operator of the pointer momentum of the photon, respectively. Here $\tau\delta(t-t_0)$ is a real function with $\int \tau\delta(t-t_0)dt = \tau$, in which τ represents the coupling strength of interaction. The effect of coupling could be described with a unitary operator $\hat{U} = \exp(-i\tau\hat{P} \otimes \hat{A})$ ($\hbar = 1$ throughout the paper). According to the formalism in the frequency-domain weak measurement [15], we consider a Mach-Zehnder interferometer with a broadband light source. As shown in Fig. 1, \hat{A} acts on the which-path space in the interferometer, and the incoming light is split into two arms by a polarization beam splitter (PBS) with different eigenstates $|\psi_r^+\rangle$ and $|\psi_r^-\rangle$. The light from the two arms is then recombined at another PBS. For the preselected pointer state $|\psi_i\rangle|\varphi\rangle$, after interaction between the system and pointer, it can be written as $\exp(-i\tau\hat{P} \otimes \hat{A})|\psi_i\rangle|\varphi\rangle$.

Projected to postselected state $|\psi_f\rangle$, the outgoing pointer state is

$$|\phi\rangle = \langle\psi_f|e^{-i\tau\hat{P}\otimes\hat{A}}|\psi_i\rangle|\varphi\rangle = \langle\psi_f|\psi_i\rangle e^{i\tau\hat{P}A_w}|\varphi\rangle \quad (1)$$

when states $|\psi_i\rangle$ and $|\psi_f\rangle$ are almost orthogonal. Referring to Ref. [22], the momentum of pointer satisfies

$$\langle\hat{P}\rangle_f = \langle\hat{P}\rangle_i + 2\tau(\text{Var}_P)\text{Im}A_w \quad (2)$$

in which we introduce the variance of momentum Var_P in the initial pointer state

$$\text{Var}_P = \langle\varphi|P^2|\varphi\rangle - (\langle\varphi|P|\varphi\rangle)^2. \quad (3)$$

In our scheme, we focus on high-sensitivity measurement of the angular rotation. The highest sensitivity can be obtained when $\hat{A} = -i|H\rangle\langle V| + i|V\rangle\langle H|$ (see the Appendix). The preselection and postselection processes can be realized through a linear polarizer. The preselection and postselection states are chosen to be $|\psi_i\rangle = (|H\rangle + |V\rangle)/\sqrt{2}$ and $|\psi_f\rangle = [\sin(\frac{\pi}{4} + \varepsilon)|H\rangle - \cos(\frac{\pi}{4} + \varepsilon)|V\rangle]/\sqrt{2}$, respectively, in Fig. 1. The weak interaction process can be described as $\hat{U} = \exp(-i\tau\hat{P} \otimes \hat{A})$, in which $\hat{A} = -i|H\rangle\langle V| + i|V\rangle\langle H|$. For simplification, the initial state of system is prepared to be a Gaussian wave function centered at P_0 (without normalized),

$$\varphi(P) = \langle\mathbf{P}|\varphi\rangle = e^{-\frac{(P-P_0)^2}{2\Delta^2}}, \quad (4)$$

where Δ is the width of the spectrum in the initial state. In weak measurement experiments with the transversal shift, the

component of momentum in the interaction is perpendicular to the direction of light. In our weak measurement scheme, the uncertainty of the perpendicular momentum is relatively small, and the momentum P of photons in the Hamiltonian is in the direction of the motion [12]. After postselection, the final state of the system is written as

$$\phi(P) = \langle\psi_f|e^{i\tau\hat{P}\otimes\hat{A}}|\psi_i\rangle\langle\mathbf{P}|\varphi\rangle = \sin(\tau P - \varepsilon)e^{-\frac{(P-P_0)^2}{2\Delta^2}}. \quad (5)$$

The probability density distribution in momentum domain is thus

$$\Phi(P) = |\phi(P)|^2 = \sin^2(\tau P - \varepsilon)e^{-\frac{(P-P_0)^2}{\Delta^2}}. \quad (6)$$

The momentum shift caused by a small time delay could be written as

$$\Delta P = \frac{\int P\Phi(P)dP}{\int \Phi(P)dP} - P_0 = \frac{2\tau\Delta^2(\tau P_0 - \varepsilon)}{\tau^2\Delta^2 + 2(\tau P_0 - \varepsilon)^2}, \quad (7)$$

$$\Delta P = \frac{2(\tau P_0 - \varepsilon)}{\tau}, \quad |\tau P_0 - \varepsilon| \ll \tau\Delta. \quad (8)$$

When the coupling interaction is weak enough ($|\Delta\tau| \ll 1$), we obtain Eq. (7). Here we consider a specific parameter regime, the inverse weak-value regime with $|\tau P_0 - \varepsilon| < \tau\Delta$ [23], and choose it as the working regime. Previous work [21] showed that WVA system obtains the highest sensitivity in the inverse weak-value regime. Specifically, we obtain Eq. (8) when $|\tau P_0 - \varepsilon| \ll \tau\Delta$. In the previous work [12,21], the coupling strength of the frequency-domain weak measurement is discrete: $\tau = n\pi/P_0$, $n = 1, 2, 3, \dots$. In contrast, there is a ε satisfying $|\tau P_0 - \varepsilon| \simeq 0$ for any small τ in our scheme, and an ultrasensitive measurement can be expected for an ultrasmall τ . On the other hand, a continuously adjustable coupling strength τ may offer an optimal $\text{Im}A_w$ in practice.

III. ULTRASENSITIVE MEASUREMENT VIA OPTICAL ROTATORY EFFECT

In Mach-Zehnder interferometer scheme, the coming light is usually split into two arms with linear polarization state $|H\rangle$ and $|V\rangle$. As proved above, to measure the angular rotation angle, $\hat{A} = -i|H\rangle\langle V| + i|V\rangle\langle H|$ is the optimum with the highest sensitivity. It can be achieved by putting a set of a HWP and a QWP before and after the interferometer to transform basis $\{|\psi_r^+\rangle, |\psi_r^-\rangle\}$ to basis $\{|H\rangle, |V\rangle\}$ and reverse it. The small time delay between the two arms transforms into the phase difference between $|\psi_r^+\rangle$ and $|\psi_r^-\rangle$. In this scheme, the coupling strength τ can be continuously adjusted, and there will be an anomalous amplification of the pointer momentum.

Here we propose a scheme to measure the optical rotation angle with quartz crystal. When the light propagates along the optical axis of quartz crystal, the optical rotation effect is dominant and the birefringent effect could be ignored, and the rotation angle relies on the momentum of photon linearly [12]. The interaction Hamiltonian of the quartz rotator can be written as $\hat{H} = \tau\hat{P} \otimes \hat{A}$ and $\tau = \alpha l/P_0$, $\hat{A} = -i|H\rangle\langle V| + i|V\rangle\langle H|$, in which α and l represent specific rotation and the thickness of crystal, respectively. Conceptually, the set of the Mach-Zehnder interferometer, HWPs, and QWPs can be replaced by quartz rotators, and the coupling strength is

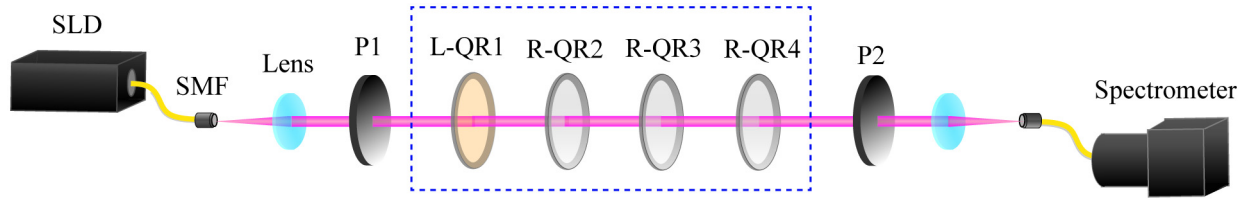


FIG. 2. Experimental configuration of optical rotation measurement. The signal beam is focused inside the optical crystal with high collimation. To set the preselection and postselection, polarizers (Thorlabs Inc., LPVIS050-MP, extinction ratio of 100 000:1) are put before and after the optical crystal and are almost orthogonal. The second polarizer is fixed in a rotation platform. The quartz rotators act as weak interaction between polarization and momentum of photons, and the rotation angle is nearly linear to the momentum of photons. Left-handed and right-handed quartz rotators are both applied in our system to achieve a tiny rotatory dispersion effect. A light source (SLD, IPSDD0804, 830 nm, 5 mW, Inphenix) and spectrograph are used in our experiment for spectral analysis.

related to thickness of crystal. The actual experimental setup is shown in Fig. 2.

The scheme of our experiment is depicted in Fig. 2. Light source (SLD, IPSDD0804, 5 mW, Inphenix) used here is centered at 830 nm with a bandwidth of 14 nm. The light is collimated by a lens and passes through quartz crystals along the optical axis. Although quartz crystal has both birefringence and optical activity, the birefringence can be ignored while light propagates along the optical axis. In this case optical activity takes effect. When light passes through quartz crystal, optical activity results in the phase difference between the circular polarization state $|\psi_r^+\rangle$ and state $|\psi_r^-\rangle$. According to the rotatory dispersion effect [24], the interaction Hamiltonian could be written as $\hat{H} = \tau \delta(t - t_0) \hat{\mathbf{P}} \otimes \hat{\mathbf{A}}$, in which $\hat{\mathbf{A}} = -i|H\rangle\langle V| + i|V\rangle\langle H|$. Polarizers (Thorlabs Inc., LPVIS050-MP, extinction ratio of 100 000:1) are set before and after the quartz crystal as preselection and postselection, and their polarization angles are nearly orthogonal. As Eq. (8) shows, a smaller τ will lead to a higher response of the center wavelength shift varying ε . Here we adopt a set of quartz rotators: one piece of 1-mm-thick left-handed quartz rotator and three pieces of 0.3-mm-thick right-handed quartz rotators. We change the couple strength by changing the number of right-handed quartz rotators and perform the measurement in a set of coupling strength with an effective thickness of $\{0.1 \text{ mm}, 0.4 \text{ mm}, 0.7 \text{ mm}, 1.0 \text{ mm}\}$ and weak value $\{57, 14.3, 8.1, \text{ and } 5.7\}$, respectively. For a fixed thickness, we set $|\tau P_0 - \varepsilon| = 0$ as the zero point and change ε by rotating the second polarizer. The shift of the center wavelength in the output spectra can be written as

$$\Delta\lambda = \Delta(2\pi/P) \approx \frac{-2\pi}{P_0^2} \Delta P = \frac{-2\pi}{P_0^2} \frac{2\tau\Delta^2(\tau P_0 - \varepsilon)}{\tau^2\Delta^2 + 2(\tau P_0 - \varepsilon)^2}. \quad (9)$$

The experimental results, along with the theoretical curves obtained by Eq. (9), are shown in Fig. 3. Around the zero point, we could find that a smaller τ leads to a higher response rate, which is reflected by the slope of curves. In our experiment, the highest response of the wavelength shift is achieved when $l = 0.1 \text{ mm}$ with an amplification factor as large as 57. In Fig. 3, the slopes of dashed black lines at zero point are 3884 nm/rad, 5494 nm/rad, 9711 nm/rad, and 38 840 nm/rad, respectively. Compared with previous work [19,20] with the highest sensitivity of 2880 nm/rad, more

than 13 times higher sensitivity was obtained. A much higher response of the wavelength shift can be expected for a smaller τ , which shows the potential of our scheme in ultrasensitive measurements.

The theoretical curves calculated from Eq. (7) show that the maximum shift is related to the bandwidth Δ in the initial state. In Fig. 3 we obtain a high correspondence between experimental results and theoretical solid curves for $l = 0.4 \text{ mm}$, 0.7 mm, and 1.0 mm. However, there are slight deviations for $l = 0.1 \text{ mm}$, and the maximum shift of wavelength is slightly bigger than theoretical result. The experiment with an effective thickness of 0.1 mm is achieved by putting one piece of 1.0-mm-thick left-handed quartz rotator and three pieces of 0.3-mm-thick right-handed quartz rotator into our system. Given the high response of wavelength shift and limited angular resolution of the rotation platform ($1'$), it is hard to locate the zero point, especially for $l = 0.1 \text{ mm}$. Here we use the theoretical results as a calibration and obtain a corrected prediction curve for $l = 0.1 \text{ mm}$, which is in conformity with data points. According to our calculations, the deviation of ε at the zero point is approximately $5.7 \times 10^{-4} \circ$.

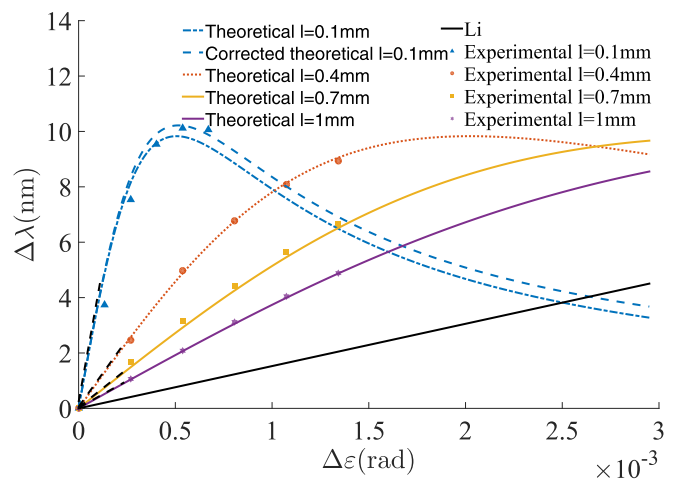


FIG. 3. Center wavelength shifts varying ε . The theoretical and experimental results are shown for four different values of effective thickness of quartz crystal. The dashed curve is the corrected curve while taking the zero point offset into account for $l = 0.1 \text{ mm}$. The sensitivity to measure ε can be characterized by the dashed black lines at zero point, and the solid black line (lowest) is the center wavelength shift in Li's scheme [19].

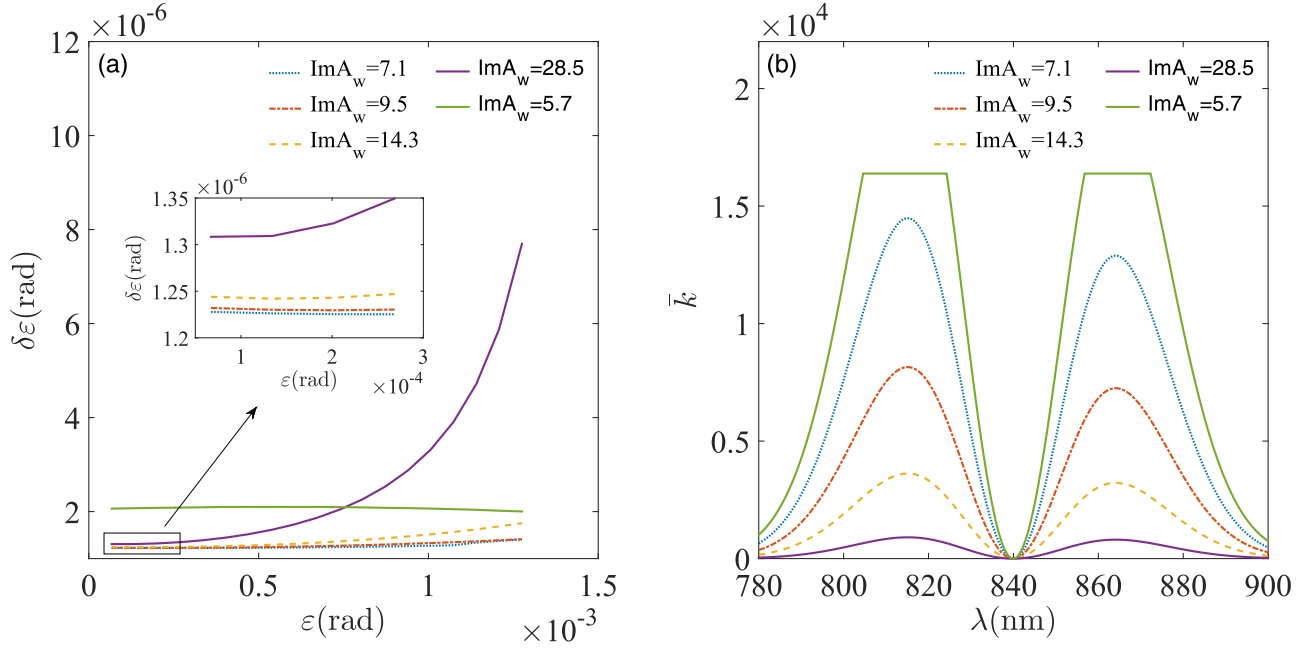


FIG. 4. Comparison between WVA with different $\text{Im}A_w$. (a) Precision obtained from CCD with saturation threshold $k_s = 16\,384$ and readout noise parameters $\mu = 6$, $\sigma_1 = 10$. The center wavelength of the input Gaussian beam is 840 nm, and the FWHM is 25 nm, carrying 10^{10} photons per exposure in average. The results show that the precision of the system is significantly reduced for $\text{Im}A_w = 5.7$. (b) The average intensity distribution of the spectrum received by the CCD for various $\text{Im}A_w$ in (a). The plot shows that saturation effects are obvious for $\text{Im}A_w = 5.7$.

IV. NOISE ANALYSIS

Despite the fact that the WVA technique does not overcome the fundamental limits in optics [20,25–28], WVA shows great potential in suppressing technical noise. A comprehensive discussion by Jordan [29] has claimed that WVA gives technical advantages for specific noise and schemes. Another important step was made as a theoretical study [30] claimed the WVA can outperform conventional measurement in the presence of detector saturation. Therefore, this section is organized as follows. First, for a noiseless light, we present that the precision of WVA is greatly affected by the saturation effect, and a continuously adjustable coupling strength promises an optimal $\text{Im}A_w$. Second, we present that WVA schemes have great performance in suppressing light intensity jitter. For an LED light source with light intensity jitter, we demonstrate that WVA with optimized $\text{Im}A_w$ has a better precision performance.

We notice that Fisher information (FI) [29,31] has been widely used in WVA. In our experiment, the detector used in the spectrometer is a high-sensitivity 3648-element CCD array (Toshiba, TCD1304AP). Assuming the total average number of photons at the input is \bar{n}_t during each exposure, the number of photons arriving on the j th array of the CCD is expected to be $\bar{n}_j^{wm} = \bar{n}_t \int_j d p(|\mathbf{P}|\phi_{wm})|^2$ and $\bar{n}_j^{cm} = \bar{n}_t \int_j d p(|\mathbf{P}|\phi_{cm})|^2$ in WVA and CM schemes, respectively. The exact number N_j of photoelectrons at the j th array of the CCD follows a probability distribution $p(N_j|\eta\bar{n}_j, X)$, in which η is the detection efficiency of the CCD and X represents all prior information. In addition, we introduce readout noise and classical noise at each array of the CCD, which follow the normal distribution $\mathcal{N}_1(\mu, \sigma_1^2)$ and Poisson distribution $p(N_j)$,

respectively. Thus, the response of the CCD can be obtained by the conditional probability distribution $P(k_j, N_j)$, where k_j is the readout at the j th array. Considering the saturation threshold k_s , the distribution at the threshold should be written as $p(k_s) = \sum_{k_j \geq k_s} p(k_j)$. Thus, the probability distribution of k_j at the j th array can be determined as follows:

$$p(k_j|X) = \sum_{N_j} p(k_j, N_j)p(N_j|\eta\bar{n}_j, X). \quad (10)$$

Therefore, the FI for rotation angle ϵ in our experiment is [29]

$$F_g(\epsilon) = \sum_j p(k_j|X) \left[\frac{\partial}{\partial \epsilon} \ln p(k_j|X) \right]^2, \quad (11)$$

where $j = \{k_1, k_2, \dots, k_M\}$ refers to the outcome of M arrays of the CCD.

More specifically, we employ center-of-mass (COM) estimation to estimate the parameter ϵ in our weak measurement scheme, which is compared with a standard polarimeter. The COM estimator can be expressed as $\Delta\lambda(\epsilon) = \frac{\sum_j (k_j - \mu)\lambda_j}{\sum_j (k_j - \mu)} - \lambda_0$, where k_j and λ_j are the number of photoelectrons and corresponding wavelength at the j th array, respectively. Therefore, the precision $\delta\epsilon$ in COM estimation can be calculated by $\delta^2\epsilon_{COM} = \sum_j \delta^2 \left[\frac{k_j - \mu}{\sum_j (k_j - \mu)} \right] \lambda_j^2 / \left(\frac{\partial \Delta\lambda}{\partial \epsilon} \right)^2$. Similarly, the polarimeter estimator can be formulated from $I(\epsilon) = \sum_j (k_j - \mu)$, and the variance of ϵ is written as $\delta^2\epsilon_{SM} = \sum_j \delta^2 k_j / \left(\frac{\partial I}{\partial \epsilon} \right)^2$.

We consider an actual camera with saturation threshold $k_s = 16\,384$ (a 2^{14} -bit camera) and readout noise parameters $\mu = 6$, $\sigma_1 = 10$. The center wavelength of the input Gaussian

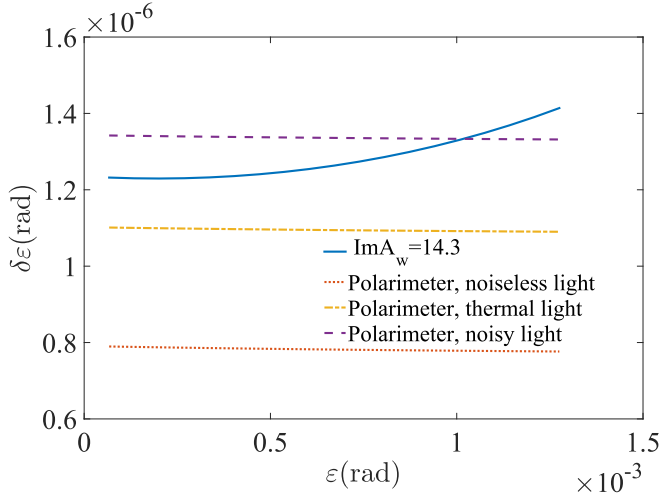


FIG. 5. Comparison between the precision of a polarimeter and that of WVA with $\text{Im}A_w = 14.3$ for three kinds of light source. The plot shows that the performance of a polarimeter is greatly affected by light intensity jitter. Although a polarimeter outperforms WVA for a classical thermal light, the output signal is similar to noisy light due to air disturbance, vibration, and so on. In this situation, WVA can outperform a polarimeter.

beam is 840 nm, and the FWHM is 25 nm. Assuming the number of input photons per exposure is approximately 10^{10} , we compare the precision of WVA with $\text{Im}A_w = 5.7, 7.1, 9.5, 14.3, 28.5$ for a noiseless light in Fig. 4(a). As shown in Fig. 4(b), the number of photons received by CCD increases as $\text{Im}A_w$ decreases. For low \bar{k} , saturation plays a minor role. Due to the intrinsic readout noise of the CCD, the system obtains a better performance of precision as $\text{Im}A_w$ decreases. For high \bar{k} , saturation compromises the performance of the system as $\text{Im}A_w$ increases. Therefore, the results show that for a specific number of input photons, there exists an optimal $\text{Im}A_w$ that can coordinate various kinds of noise and saturation effects of a particular photodetector.

In Fig. 5 we choose a polarimeter as conventional measurement and plot the precision of polarimeter and WVA with $\text{Im}A_w = 14.3$ for three kinds of light sources. To analyze the effect of light intensity jitter on WVA and a polarimeter, we assume three photon number probability distributions: $p(N_j|\eta\bar{n}_j, X) = \delta(N_j - \eta\bar{n}_j)$ for noiseless light, $p(N_j|\eta\bar{n}_j, X) = (2/\eta\bar{n}_j)^2 \exp(-2N_j/\eta\bar{n}_j)$ for thermal light, and $p(N_j|\eta\bar{n}_j, X) = \mathcal{N}(\eta\bar{n}_j, 2\eta\bar{n}_j)$ for noisy light. For the polarimeter, its precision has a strong correlation with the probability distribution of input photons [32], and fluctuations in the number of photons inhibit the performance of the system, as shown in Fig. 5. On the other hand, the precision of WVA can be simplified as $\delta\varepsilon = \sqrt{\text{Var}(\phi(\lambda))/\sum_j N_j/|\frac{\partial\Delta\lambda}{\partial g}|}$ when readout noise and saturation effects can be ignored. Here $\text{Var}(\phi(\lambda))$ is the variance of output beam spectral distribution, and it is not affected by light intensity jitter. We note that WVA does not outperform a polarimeter for ideal thermal light. However, there are many other factors in the experiment that can cause light intensity jitter, such as air disturbance, vibration, and temperature, which causes the actual situation

to be similar to noisy light. In this situation, it makes WVA advantageous to a polarimeter.

Finally, we compare the precision of a polarimeter and WVA with the identical measurement system. For the polarimeter, we remove all the quartz rotators in Fig. 2. The experiments are performed based on the setup depicted in Fig. 2, and we obtain different numbers of input photons by changing the integration time. In Fig. 6 the integration time of CCD is 4×10^{-3} s and 1.5×10^{-2} s, respectively. As Fig. 6(a) shows, the CCD detector is not saturated for WVA with various $\text{Im}A_w$. Although the WVA scheme can suppress light intensity jitter, its precision is still severely limited by the intrinsic readout noise of CCD for a scheme with large $\text{Im}A_w$ and low intensity. In this situation, a WVA scheme with $\text{Im}A_w = 57$ still cannot outperform a polarimeter. However, the scheme with optimized $\text{Im}A_w = 14.3$ can outperform a polarimeter due to light intensity jitter. Figure 6(b) demonstrates that the effects of saturation can inhibit the performance of the WVA scheme. CCD saturates when $\text{Im}A_w = 5.7$ and 8.1 , and the precision of WVA with $\text{Im}A_w = 14.3$ is about two times higher than that of $\text{Im}A_w = 5.7$ and 8.1 . In our scheme, we can obtain a continuously adjustable $\text{Im}A_w$ and provide an optimal $\text{Im}A_w$ to achieve a higher precision due to the trade-off between various kinds of technical noise and saturation effects. Figure 6(a) shows that the highest precision of WVA with optimized $\text{Im}A_w$ is about three times higher than that of a polarimeter. Currently, when the integration time is 1.5×10^{-2} s and $\text{Im}A_w = 14.3$, we obtain the precision of 6.1×10^{-7} rad for WVA. To date, more elaborated methods have been developed to measure angular rotation, such as photoelastic modulation [7] and the homodyne waveguide phase modulation [33] in the heterodyne system. Technical noise is suppressed through the analysis of periodic signals, and a precision of 6.3×10^{-7} rad is obtained, which is close to that of WVA.

V. DISCUSSION AND CONCLUSION

In conclusion, we propose a frequency-domain WVA scheme and perform an ultrasensitive measurement via the rotatory dispersion effect. Our scheme obtains a continuously adjustable coupling strength, and its sensitivity outperforms previous work by one order of magnitude. We study the effects of saturation and intrinsic noise of CCD and show that an optimal $\text{Im}A_w$ may exist in practice. We also demonstrate that WVA with optimized $\text{Im}A_w$ can outperform conventional measurement in the presence of various kinds of noise. The simplicity of our scheme shows its applicability in other frequency-domain WVA systems and potentials in ultrasensitive measurements.

ACKNOWLEDGMENTS

This research was made possible with the financial support from Science and Technology Research Program of Shenzhen City (JCYJ20170412171856582, JCYJ20170817111912585), National Science Foundation of China (NSFC) (61875102, 61675113) and Overseas Cooperation Foundation, Graduate School at Shenzhen, Tsinghua University (HW2018007).

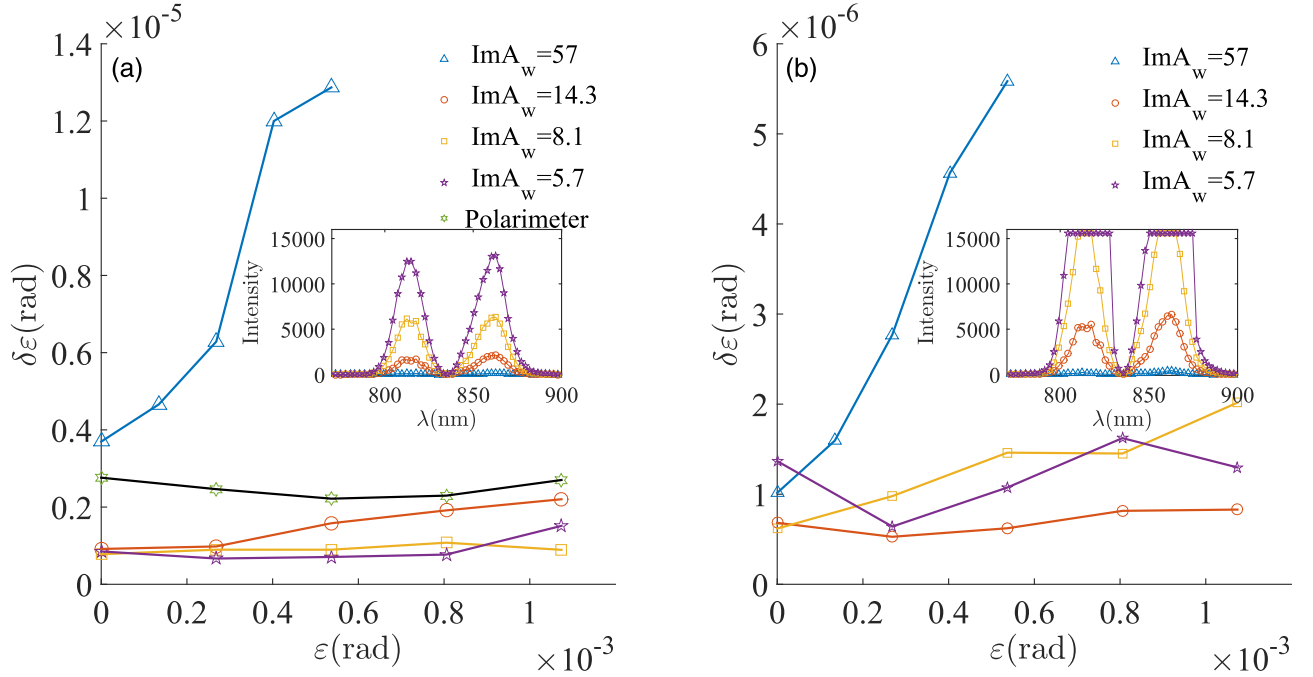


FIG. 6. Experimental results of a polarimeter and WVA with various $\text{Im}A_w$. The experiments are performed based on the above setup. (a) The integration time of CCD is 4×10^{-3} s. As the inserted picture shows, saturation is negligible for all $\text{Im}A_w$. The plot shows that WVA obtains similar precision for high \bar{n} . For low \bar{n} , intrinsic readout noise of CCD restricts the performance of the system. (b) The integration time of CCD is 1.5×10^{-2} s. As the inserted picture shows, saturation is non-negligible for $\text{Im}A_w = 8.1$ and $\text{Im}A_w = 5.7$. As \bar{n} increases, saturations restrict further improvements of precision.

APPENDIX: GENERALIZED FRAMEWORK

WVA is known for its significant amplification for parameter estimation. To obtain the highest response to rotation angle ϵ , without loss of generality, we choose a preselected state $|\psi_i\rangle$ and postselected state $|\psi_f\rangle$ with polarizers and wave plates:

$$\begin{aligned} |\psi_i\rangle &= \cos\theta|H\rangle + \sin\theta|V\rangle, \\ |\psi_f\rangle &= \sin(\theta + \delta)e^{i\varphi/2}|H\rangle - \cos(\theta + \delta)e^{-i\varphi/2}|V\rangle, \end{aligned} \quad (\text{A1})$$

where θ , $\theta + \delta + \pi/2$ are directions of two polarizers, and φ is the phase difference between states $|H\rangle$ and $|V\rangle$. Here we define that $|H\rangle$, $|V\rangle$ represent horizontal and vertical polarization states, respectively, and they are eigenstates of operator $\hat{\sigma}_z$. We focus on the condition that $\delta, \varphi \ll 1$. Generally the eigenstates $|\psi_r^+\rangle, |\psi_r^-\rangle$ of $\hat{\mathbf{A}} = |\psi_r^+\rangle\langle\psi_r^+| - |\psi_r^-\rangle\langle\psi_r^-|$ can be written as

$$\begin{aligned} |\psi_r^+\rangle &= \cos\frac{\beta}{2}|H\rangle + \sin\frac{\beta}{2}e^{i\alpha}|V\rangle, \\ |\psi_r^-\rangle &= \sin\frac{\beta}{2}e^{-i\alpha}|H\rangle - \cos\frac{\beta}{2}|V\rangle, \\ |\psi_i\rangle &= a|\psi_r^+\rangle + b|\psi_r^-\rangle, \\ |\psi_f\rangle &= c|\psi_r^+\rangle + d|\psi_r^-\rangle, \end{aligned} \quad (\text{A2})$$

where (α, β) is the azimuthal angle in a Bloch sphere. We have $a = \langle\psi_r^+|\psi_i\rangle$, $b = \langle\psi_r^-|\psi_i\rangle$, $c = \langle\psi_r^+|\psi_f\rangle$, $d = \langle\psi_r^-|\psi_f\rangle$. Hence the imaginary part of A_w is

$$\text{Im}A_w = \text{Im} \frac{ac^* - bd^*}{ac^* + bd^*}. \quad (\text{A3})$$

For further simplification, we set $\theta = \pi/4$, and by first-order approximation, Eq. (A3) can be rewritten as

$$\text{Im}A_w = \frac{2\varphi\cos\beta - 4\delta\sin\beta\sin\alpha}{4\delta^2 + \varphi^2}. \quad (\text{A4})$$

Here we focus on the measurement of rotation angle δ ; the derivative of δ is

$$\begin{aligned} \Re(\alpha, \beta, \delta, \varphi) &= \frac{\partial \text{Im}A_w}{\partial \delta} \\ &= \frac{4\sin\beta\sin\alpha(4\delta^2 - \varphi^2) - 16\delta\varphi\cos\beta}{(4\delta^2 + \varphi^2)^2}. \end{aligned} \quad (\text{A5})$$

To obtain the highest response to δ , we require that the partial derivatives of $\Re(\alpha, \beta, \delta, \varphi)$ with respect to α, β, φ satisfy that

$$\frac{\partial \Re(\alpha, \beta, \delta, \varphi)}{\partial x_i} = 0 \quad (x_i = \alpha, \beta, \varphi). \quad (\text{A6})$$

Assuming that $\varphi = m\delta$, the extrema of $\Re(\alpha, \beta, \delta, \varphi)$ can be obtained when $m = 0, \alpha = \beta = \pi/2$, which is the optimum to measure angular rotation. At this point we have

$$\begin{aligned} |\psi_r^+\rangle &= \frac{1}{\sqrt{2}}(|H\rangle + i|V\rangle), \\ |\psi_r^-\rangle &= \frac{1}{\sqrt{2}}(|H\rangle - i|V\rangle), \end{aligned} \quad (\text{A7})$$

$$\hat{\mathbf{A}} = -i|H\rangle\langle V| + i|V\rangle\langle H|.$$

Hence, $\text{Im}A_w = -1/\delta$, and the highest sensitivity can be obtained to measure the angular rotation angle. According to Eq. (A7), the eigenstates $|\psi_r^+\rangle, |\psi_r^-\rangle$ of $\hat{\mathbf{A}}$ are circular

polarizations. Analogously, based on Eq. (A4), the optimum condition to measure phase difference φ is $\alpha = \beta = 0$, $\delta = 0$. Here we get $\hat{A} = |H\rangle\langle H| - |V\rangle\langle V|$, which is con-

sistent with previous work [12]. Therefore, Eq. (A4) offers a general weak measurement theory for various parameter estimation.

-
- [1] J. Dai, N. Karpowicz, and X.-C. Zhang, *Phys. Rev. Lett.* **103**, 023001 (2009).
- [2] N. Hur, S. Park, P. Sharma, J. Ahn, S. Guha, and S.-W. Cheong, *Nature (London)* **429**, 392 (2004).
- [3] M. Hallaji, A. Feizpour, G. Dmochowski, J. Sinclair, and A. M. Steinberg, *Nat. Phys.* **13**, 540 (2017).
- [4] E. Zavattini, G. Zavattini, G. Ruoso, E. Polacco, E. Milotti, M. Karuza, U. Gastaldi, G. Di Domenico, F. Della Valle, R. Cimino *et al.*, *Phys. Rev. Lett.* **96**, 110406 (2006).
- [5] P.-F. Li, Y.-Y. Tang, Z.-X. Wang, H.-Y. Ye, Y.-M. You, and R.-G. Xiong, *Nat. Commun.* **7**, 13635 (2016).
- [6] A. Basiri, X. Chen, J. Bai, P. Amrollahi, J. Carpenter, Z. Holman, C. Wang, and Y. Yao, *Light: Sci. Appl.* **8**, 78 (2019).
- [7] K.-W. Li, Z.-B. Wang, L.-M. Wang, and R. Zhang, *J. Opt. Soc. Am. A* **33**, 2041 (2016).
- [8] J.-Y. Lin, K.-H. Chen, and D.-C. Su, *Opt. Commun.* **238**, 113 (2004).
- [9] Y. Aharonov, D. Z. Albert, and L. Vaidman, *Phys. Rev. Lett.* **60**, 1351 (1988).
- [10] O. Hosten and P. Kwiat, *Science* **319**, 787 (2008).
- [11] G. I. Viza, J. Martínez-Rincón, G. A. Howland, H. Frostig, I. Shomroni, B. Dayan, and J. C. Howell, *Opt. Lett.* **38**, 2949 (2013).
- [12] X.-Y. Xu, Y. Kedem, K. Sun, L. Vaidman, C.-F. Li, and G.-C. Guo, *Phys. Rev. Lett.* **111**, 033604 (2013).
- [13] H. Li, Y. Li, J.-Z. Huang, M. Liu, and G. Zeng, *Appl. Phys. Lett.* **114**, 161906 (2019).
- [14] D. J. Starling, P. B. Dixon, A. N. Jordan, and J. C. Howell, *Phys. Rev. A* **80**, 041803(R) (2009).
- [15] N. Brunner and C. Simon, *Phys. Rev. Lett.* **105**, 010405 (2010).
- [16] Y. Kedem, *Phys. Rev. A* **85**, 060102(R) (2012).
- [17] S. Pang, J. R. G. Alonso, T. A. Brun, and A. N. Jordan, *Phys. Rev. A* **94**, 012329 (2016).
- [18] X. Qiu, L. Xie, X. Liu, L. Luo, Z. Zhang, and J. Du, *Opt. Lett.* **41**, 4032 (2016).
- [19] D. Li, Y. He, Y. Ruan, Q. Lin, and K. Li, *J. Phys. D* **52**, 475401 (2019).
- [20] Y.-J. Zhang, L.-X. Shi, Y. Xu, X. Zheng, J.-W. Li, Q. Wu, S.-X. Li, and Y.-H. He, *Opt. Express* **27**, 9330 (2019).
- [21] Y. Xu, L. Shi, T. Guan, C. Guo, D. Li, Y. Yang, X. Wang, L. Xie, Y. He, and W. Xie, *Opt. Express* **26**, 21119 (2018).
- [22] R. Jozsa, *Phys. Rev. A* **76**, 044103 (2007).
- [23] J. Dressel, K. Lyons, A. N. Jordan, T. M. Graham, and P. G. Kwiat, *Phys. Rev. A* **88**, 023821 (2013).
- [24] S. Chandrasekhar, *Proc. R. Soc. London, Ser. A* **259**, 531 (1961).
- [25] P. B. Dixon, D. J. Starling, A. N. Jordan, and J. C. Howell, *Phys. Rev. Lett.* **102**, 173601 (2009).
- [26] A. Feizpour, X. Xing, and A. M. Steinberg, *Phys. Rev. Lett.* **107**, 133603 (2011).
- [27] C.-F. Li, X.-Y. Xu, J.-S. Tang, J.-S. Xu, and G.-C. Guo, *Phys. Rev. A* **83**, 044102 (2011).
- [28] S. Wu and Y. Li, *Phys. Rev. A* **83**, 052106 (2011).
- [29] A. N. Jordan, J. Martínez-Rincón, and J. C. Howell, *Phys. Rev. X* **4**, 011031 (2014).
- [30] J. Harris, R. W. Boyd, and J. S. Lundeen, *Phys. Rev. Lett.* **118**, 070802 (2017).
- [31] L. Xu, Z. Liu, A. Datta, G. C. Knee, J. S. Lundeen, Y.-Q. Lu, and L. Zhang, *Phys. Rev. Lett.* **125**, 080501 (2020).
- [32] J. W. Goodman, *Statistical Optics* (John Wiley & Sons, New York, 2015).
- [33] R.-C. Twu, K.-W. Wang, and H.-Y. Tu, *Sens. Actuators B* **249**, 725 (2017).